Insights into pore surface modification of mesoporous polymer–silica composites: introduction of reactive amines†

Rémy Guillet-Nicolas, Louis Marcoux and Freddy Kleitz*

Received (in Gainesville, FL, USA) 11th September 2009, Accepted 12th November 2009
First published as an Advance Article on the web 12th January 2010
DOI: 10.1039/b9nj00478e

Pore surface engineering of mesoporous materials is fundamental for the development of highly selective sorbents, solid catalysts or drug delivery systems. In the present study, tailored mesoporous amine-functionalized polymer–silica composites are synthesized using a two-step *mesopore surface-confined* polymerization technique. For this, a functional polymer, polychloromethylstyrene (PCMS), is first introduced as a uniform coating on the mesopore surface of mesoscopically ordered silica, *e.g.* SBA-15 or KIT-6 materials. In the second step, selected amines, as model functions, are attached to the polymer surface by nucleophilic substitution, generating a variety of nanoporous amino-polymer–silica composites. In particular, it is shown that this approach allows for a tuning of surface concentration of the organic groups either by varying polymer loading or by copolymerization of the CMS monomers with non-reactive monomers (styrene). Moreover, this method is suitable for facile introduction of diverse types of amine groups, *e.g.* secondary amines, diamines, linear or branched polyamines. The pristine mesoporous silica hosts and the different functional mesoporous polymer–silica composites are characterized in detail by nitrogen physisorption, powder X-ray diffraction, elemental analysis, thermogravimetry–differential thermal analysis coupled with mass spectrometry (TG-DTA/MS), attenuated total reflection-IR spectroscopy (ATR-IR) and scanning electron microscopy. In addition, the obtained functionalized mesoporous composites are proven active as base catalysts in the Knoevenagel condensation. From these investigations, it appeared that the preparation method should be highly flexible and appropriate to enable modulation of location and distribution of various functional groups within mesopores.

Introduction

In general, ordered mesoporous silica materials[1–3] exhibit high specific surface area, high pore volume, and readily tuneable pore size in the nanometer range (2–15 nm). Nevertheless, efficient modification of the pore surface of mesoporous silica is often the crucial step towards the design of functional materials[4–8] and consequently, functionalization methods, *e.g.* post-synthetic grafting, co-condensation methods, encapsulation, *etc.*, are attracting tremendous interest.[9–14] As one new strategy to incorporate organic functionalities within such mesoporous hosts, the *pore surface-confined* polymerization approach that was recently reported by Choi *et al.*[15] is gaining increasing attention.[16–22] In contrast to previous methods based on growing polymers inside the pores of mesoporous silica, which often led to severe pore blocking,[23–31] this alternative approach enabled the retention of the high porosity of the robust inorganic mesostructured materials, *e.g.* SBA-15 or KIT-6 silicas,[2,32] while simultaneously associating the vast functionalization possibilities of organic polymer chemistry. In this system, a mixture of monomer, cross-linker, and radical initiator is first introduced inside the pores of a suitable mesoporous host (*e.g.* SBA-15-type silica) using the incipient-wetness technique. Subsequently, radical polymerization is thermally initiated to generate a fully integrated mesoporous polymer–silica composite, the polymer being present as a thin uniform layer on the internal pore surface. The thus-prepared nanocomposites usually exhibit high surface areas (*ca.* 350–600 $m^2\ g^{-1}$) and functionalized mesopore surfaces which remain fully accessible. Although functionalities may be introduced into mesoporous silica by other means, such as grafting or co-condensation methods, the above technique of polymer coating can offer some valuable advantages. In particular, the physical and chemical properties of the functional mesopore surface coating can easily be tailored by changing the nature of the polymer (hydrophobic, hydrophilic, based on chemically or physically active monomers, *etc.*), by varying the thickness of the coating, or by changing the degree of polymer cross-linking (thus modulating swelling ability and

Canada Research Chair on Functional nanostructured materials, Department of Chemistry, Université Laval, Québec, Canada G1V 0A6. E-mail: freddy.kleitz@chm.ulaval.ca; Fax: +1 418 656 7916; Tel: +1 418 656 7812

† Electronic supplementary information (ESI) available: Experimental section and optimisation conditions for the amination. Physico-chemical characteristics derived from N_2 sorption for the EDA-PCMS composites prepared with different polymer locations. Catalytic recycling tests. N_2 sorption isotherms of EDA-PCMS(30)-KIT-6 and EDA-PCMS:PS composites. TGA of PCMS(30)-SBA-15 composite before and after treatment with EDA. ATR-FTIR spectra of the KIT-6-derived materials and copolymer composites. Time-course of Knoevenagel condensation catalyzed by amino-functionalized composites with different amine-to-reagents ratios. See DOI: 10.1039/b9nj00478e

surface site accessibility). Moreover, copolymerization is possible to selectively combine different monomers, and subsequent post-grafting of functional groups can also be performed, avoiding here the use of any costly silane reagents. Concerning the development of this new family of porous nanocomposites, further investigations are nevertheless still needed regarding the different possibilities of mesopore surface (post)functionalization, their chemical reactivity and catalytic behavior. In particular, the selective pore surface introduction of base functionalities remains to be explored as such functional nanoporous polymer–silica systems could be of great interest for liquid phase heterogeneous catalysis and drug delivery applications. Here, amine groups, especially, are attractive for applications in base catalysis,[33–42] CO_2 capture,[43–45] scavenging of heavy metal cations[46–48] or as binding sites for bioactive molecules and controlled drug release.[49–52]

In this contribution, we now study in detail the synthesis of amine-functionalized mesoporous polymer–silica composites generated through post-synthesis attachment of amine groups on the pore surface of polymer coated mesoporous silica. The functional nanocomposites are characterized by N_2 physisorption, low-angle powder XRD, thermogravimetry coupled with mass spectrometry, ATR-IR, elemental analysis, scanning electron microscopy and titration. The results demonstrate controlled inclusion of various amine groups on the mesopore surface of the materials with tailored quantity and density of amine sites. It is shown that the functionalization approach allows for a fine-tuning of surface concentration of amine groups by: (1) changing the type of amine, (2) varying the loading in polymer, and (3) performing copolymerization of CMS monomers with non-reactive monomers. Base catalysis properties of these new materials were also evaluated by testing their performance in the Knoevenagel condensation serving as a model generic reaction. The properties of the functionalized mesoporous materials are compared in terms of loadings and positioning of the functional groups.

Experimental section

Materials

Preparation of the mesoporous polymer–silica nanocomposites. First, the syntheses of the mesoporous silica hosts (*e.g.* SBA-15 and KIT-6) were performed at low acidic concentrations (0.3–0.5 M HCl) following reported procedures,[32,53,54] as detailed in ESI.† Various loadings in weight% of cross-linked polychloromethylstyrene, PCMS, could then be introduced inside the pores of the above silicas following the original procedure reported by Choi *et al.*[15] In our case, chloromethylstyrene, CMS (Aldrich, 90%), divinylbenzene, DVB (Aldrich, 80%), and benzoyl peroxide, BPO (Aldrich, 97%, recrystallized in acetone), were used as reactive monomer, cross-linker, and radical initiator, respectively. Typically with 30 wt% of polymer, 0.228 mL (1.6 mmol) CMS, 0.058 mL (0.4 mmol) DVB and 17.7 mg (0.07 mmol) of BPO were dissolved in 1.96 mL CH_2Cl_2. This solution was then introduced in 1 g of SBA-15 silica (dried overnight at 150 °C under vacuum) using the incipient-wetness technique. The impregnated material was then dried for 4 h at 40 °C to remove CH_2Cl_2 and then subjected to three vacuum–freeze–thaw cycles using acetone–dry ice mixture as a coolant. The material was left under vacuum at 35 °C for 6 h to facilitate diffusion of the organics within the pores. Subsequently, polymerization was performed under reduced pressure triggered by thermal treatment at 60 °C for 6 h, followed by 100 °C for 1 h and 120 °C for 1 h. The resulting composites were washed with $CHCl_3$ and EtOH, filtered, and dried at 80 °C for 24 h. Alternatively, a series of PCMS–SBA-15 composites with lower concentration of reactive sites (*i.e.* *diluted* sites) have also been prepared. For this, different molar quantities of CMS were replaced by styrene (Alfa Aesar, 99%). In a typical copolymer material synthesis, 0.131 mL (0.93 mmol) CMS was mixed with 0.107 mL (0.93 mmol) styrene, 0.066 mL (0.46 mmol) DVB, 20.3 mg (0.08 mmol) BPO and 1.96 mL CH_2Cl_2. The rest of the procedure followed the steps described previously. For comparison purpose, PCMS–SBA-15 composites with the polymer being incorporated randomly inside the mesopores were also prepared.[15] For the synthesis, the preparation procedure was the same as before, except that CH_2Cl_2 was replaced by toluene for the impregnation step. The samples are denoted PCMS(x), where x represents the initial polymer loading in wt% introduced in the composite. The copolymerized materials are denoted PCMS(a; x), where a represents the CMS/styrene molar ratio ($0 < a < 1$). The materials prepared with randomly incorporated polymer are denoted PCMS-R.

Preparation of the amino-PCMS composites. All amines were used as received without further purification. For the procedure with ethylenediamine (EDA),[55,56] 200 mg of dried PCMS–SBA-15 powder were dispersed in 20 mL of acetonitrile, and 0.075 g (1.25 mmol) of EDA (99%, Alfa-Aesar) was added to this suspension, which corresponds to an EDA/CMS molar ratio of 5 (see Table S1 (ESI†) for optimization conditions). The mixture was stirred at 60 °C for 24 h. The material was then filtered, washed with EtOH and acetone and dried in vacuum at 80 °C for 24 h. The resulting materials are denoted EDA–PCMS(x). Using a similar procedure, tris(2-aminoethyl)amine, TAEA (96% Aldrich), triethylenetetramine, TETA (60% Aldrich), diethylenetriamine, DETA (99% Aldrich), and butylamine, BA (99.5% Aldrich), have also been fixed to the polymer surface. Finally, a physical mixture of SBA-15 and EDA–PCMS, denoted EDA–PCMS-M, was also prepared. Here, bulk PCMS with 20% cross-linking was synthesized[57] and treated with EDA under the same conditions as previously mentioned. The bulk EDA–PCMS was then mixed with pure silica SBA-15, in the same polymer–silica proportion as the coated composites.

Characterization methods

Nitrogen sorption isotherms were measured at −196 °C on a Quantachrome Autosorb 1-C instrument. The silica materials were outgassed under vacuum at 200 °C for 16 h prior to measurement, while the composite samples were outgassed at 80 °C for 16 h. Specific surface area, S_{BET}, was determined using the BET equation in the range $0.05 \geq P/P_0 \geq 0.20$, and total pore volume was obtained at $P/P_0 = 0.95$. The pore

size distributions were determined by using non-local density functional (NLDFT) methods considering sorption of nitrogen at −196 °C in cylindrical silica pores.[58,59] Both the kernel of equilibrium NLDFT isotherms (desorption branch) and the kernel of (metastable) NLDFT adsorption isotherms (adsorption branch) were applied for pore width determination.[60] Silica micropore volumes were obtained from NLDFT cumulative pore volumes estimated for pores smaller than 2 nm. TG-DTA/MS measurements were performed using a Netzsch STA 449C thermogravimetric analyser coupled with a Netzsch Aelos QMS 403C mass spectrometer. Analyses were carried out under air flow at a heating rate of 10 °C min^{-1}. Low-angle XRD measurements were performed on a Bruker AXS Discover D8 system equipped with a Hi-Star 2D-detector and a Turbo source using CuK_{α} radiation operated at 4.5 kW. Elemental analysis was performed on a Carlos Erba 1106 Elemental Analyser. FTIR-ATR spectra were recorded using a Nicolet Magna FTIR spectrometer with a narrow band MCT detector and a diamond ATR Golden-Gate accessory (Specac Ltd., London). The spectra were obtained from 128 scans with a 4 cm^{-1} resolution. Scanning electron microscopy images were obtained with a JEOL model 840-A microscope operated at 15 kV.

Base catalysis tests

In a typical Knoevenagel condensation test, 5 mmol of both benzaldehyde (Aldrich, 99%) and ethyl cyanoacetate (Aldrich, 98%) were mixed in 35 mL toluene and heated at 80 °C. 50 mg of catalyst dried overnight at 80 °C were then introduced into the reaction vessel, which corresponds to a nitrogen/reagent ratio ranging between 0.6–2.1%, depending on the nitrogen content of the catalyst. Note that stirring rates were varied between 300 and 1000 rpm and no differences in the conversion were observed. After reaction, the catalyst was recovered by hot filtration, washed with toluene and ethanol, and dried at 80 °C under vacuum for 24 h. All catalysis tests were analyzed by gas chromatography (GC) performed on a HP 5890 equipped with a HP 5989A mass spectrometer. Conversions and selectivity were determined by GC-MS, and hexadecane was used as an internal standard.

Results and discussion

Choice of the mesoporous silica hosts

High quality SBA-15 and KIT-6 were used in this study because of their large pore sizes (>6 nm) suitable for the insertion of a polymer coating in the mesopores without causing severe pore blocking. In addition, the presence of complementary intrawall porosity in these materials[61] is beneficial for the positioning of the polymer coating. The syntheses of the pristine mesoporous silica matrices were performed under low acidic concentrations[32,53,54,62] (0.3–0.5 M HCl) to ensure excellent reproducibility, high yields of mesostructured material and high phase purity for the silica host matrix. Furthermore, the low acid concentration regimes generally allow for an efficient fine-tuning of the intrawall porosity,[53,63] which is the determining factor in the preparation of the mesoporous polymer–silica composite materials.[15,64] The nitrogen physisorption isotherms measured at −196 °C for the SBA-15 and KIT-6 hosts are presented in Fig. 1. As can be seen, the materials exhibit type IV isotherms with a sharp H1 hysteresis loop at high relative pressures, characteristic of mesostructured solids with large uniform cylindrical mesopores.[58,59,65] The periodic mesoscale organization of SBA-15 and KIT-6 was further confirmed by low-angle XRD diffraction (see Fig. 2 for SBA-15) and TEM investigations (not shown). The physicochemical parameters derived from nitrogen physisorption and XRD analyses are grouped in Table 1. The NLDFT pore size is evaluated at 8.1 nm for SBA-15 prepared with aging at 100 °C for 48 hours and the total pore volume of this sample is 1.20 cm^3 g^{-1}. The KIT-6 silica host material prepared at 100 °C for 48 hours exhibits a slightly higher pore volume, with wider mesopores of 8.8 nm (NLDFT equilibrium model). The pore volume associated with micropores (pore below 2 nm) is about 0.07 cm^3 g^{-1} for the SBA-15 sample and 0.04 cm^3 g^{-1} for the KIT-6 sample.

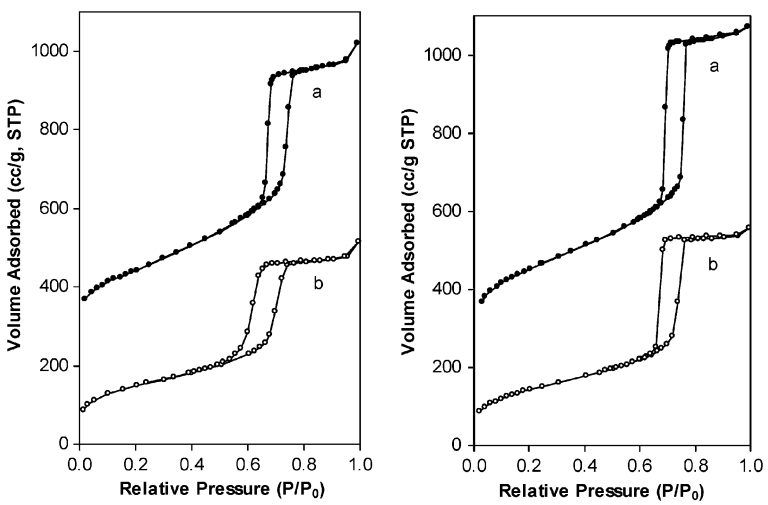

Fig. 1 (Left) N_2 adsorption–desorption isotherms measured at −196 °C for SBA-15 (offset: 200 cm^3 g^{-1}) (a) and PCMS(30)–SBA-15 (b); (right) N_2 adsorption–desorption isotherms of KIT-6 (offset: 200 cm^3 g^{-1}) (a) and PCMS(30)–KIT-6 (b).

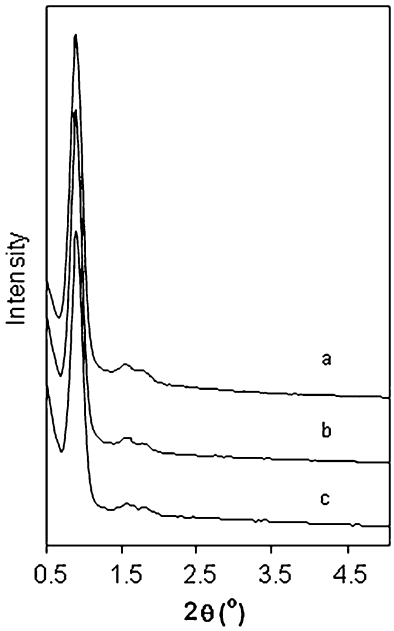

Fig. 2 Low angle powder X-ray diffraction patterns of (a) SBA-15, (b) PCMS(30)–SBA-15 and (c) EDA–PCMS(30)–SBA-15.

Synthesis of the polymer coating on the mesopore surface

PCMS was chosen as the functional polymer because it enables preparation of a variety of different functional materials from the same starting composite by the simple nucleophilic substitution of the chlorine group. The principle of the polymer insertion as a thin coating confined to the mesopore surface is illustrated in Scheme 1. A dried silica host is first impregnated with a pre-prepared mixture of the monomer, a suitable cross-linker and the radical initiator, BPO in this case, dissolved in a small quantity of a volatile solvent (dichloromethane). The incipient-wetness technique, which is followed by solvent removal and subsequent vacuum–freeze–thaw cycles, is adequate to create uniform coatings of various polymers on the mesopores surface of SBA-15. This sequence is followed by thermal polymerization of the monomers, triggered while these are being adsorbed on the pore surface. As a result, the organic polymeric thin coating remains located selectively on the mesopore surface, avoiding pore blocking. The physicochemical parameters of the resulting mesoporous PCMS–SBA-15 materials derived from N_2 sorption, powder XRD and thermogravimetric analysis are listed in Table 1. Unit cell parameters determined from XRD (Fig. 2) are presented in Table 1 and in all cases, no change in the unit cell dimension was observed after polymer insertion. This is expected since only distribution of matter in the unit cell will change and not the interplanar distances. SEM investigations (Fig. 3) revealed no bulk polymer formation after polymer incorporation. The materials are similar in terms of particle size and shape and show identical surface features. In general, the yields in polymerization (initiated with BPO) as estimated by thermogravimetric analysis are high, ranging from 88 to 95%. The sorption isotherms of the mesoporous nanocomposites prepared with 30 wt% of initial loading of monomers introduced into SBA-15 and KIT-6 are shown in Fig. 1. In addition, the nitrogen sorption isotherms obtained for three PCMS–SBA-15 samples prepared with polymer loadings of 10, 30 and 40 wt% are compared in Fig. 4. Obviously, specific adsorption capacities are substantially reduced due to the addition of the polymer which contributes to the total mass but not to the volume. However, type IV isotherms with H1 hysteresis loop indicate that the cylindrical geometry is generally maintained after PCMS insertion, pointing to uniform polymer coating inside the mesoporous channels. A systematic reduction in mean pore diameter, pore volume and specific surface area is

Table 1 Physicochemical parameters derived from N_2 sorption measurements and combustion elemental analysis for aminated polymer–silica composites

Materials	BET/ $m^2\ g^{-1}$	Pore volume[a]/ $cm^3\ g^{-1}$	a_0/nm	BJH_{ads}[b] pore size/nm	DFT_{des}[c] pore size/nm	DFT_{ads}[d] pore size/nm	Organic content[e] (%)	N content[f]/ mmol g^{-1}	
								Theo.	Expt.
SBA-15	856	1.20	11.3	8.2	8.1	7.6	—	—	—
PCMS(10)–SBA-15	683	0.95	11.3	7.8	7.9	7.5	7	—	—
EDA–PCMS(10)	553	0.86	11.3	7.3	7.3	7.3	12	0.9	1.0
PCMS(30)–SBA-15	533	0.74	11.3	7.3	7.0	7.0	23	—	—
EDA–PCMS(30)	351	0.61	11.3	6.8	6.3	7.0	25.2	2.3	2.1
PCMS(40)–SBA-15	404	0.55	—[g]	7.3	6.1	7.0	28	—	—
EDA–PCMS(40)	365	0.51	—[g]	6.9	5.5	6.8	32	3.0	2.6
PCMS(50)–SBA-15	410	0.54	—[g]	7.3	5.7	7.0	31	—	—
EDA–PCMS(50)	268	0.38	—[g]	6.8	5.5	6.8	35.5	3.4	2.6
KIT-6	913	1.32	22.5	8.6	8.8	8.1	—	—	—
PCMS(30)–KIT-6	523	0.83	22.5	8.5	8.1	7.6	20	—	—
EDA–PCMS(30)–KIT-6	456	0.72	22.5	7.3	7.6	7.0	24	2.1	1.7
PCMS(0.5; 30)–SBA-15	507	0.73	11.3	7.2	6.3	7.0	22	—	—
EDA–PCMS(0.5; 30)	446	0.66	11.3	6.8	5.9	6.8	23.5	1.2	1.3
PCMS(0.1; 30)–SBA-15	567	0.88	11.3	7.6	7.3	7.3	21	—	—
EDA–PCMS(0.1; 30)	494	0.76	11.3	7.3	7.3	7.3	23	0.2	0.6

[a] Determined at $P/P_0 = 0.95$. [b] Determined by the BJH algorithm using the adsorption branch. [c] Determined by NLDFT method taking into account the desorption branch (NLDFT equilibrium model). [d] Determined by NLDFT method taking into account the adsorption branch (NLDFT metastable adsorption branch model). [e] Determined by TG. [f] From combustion elemental analysis. [g] Not measured.

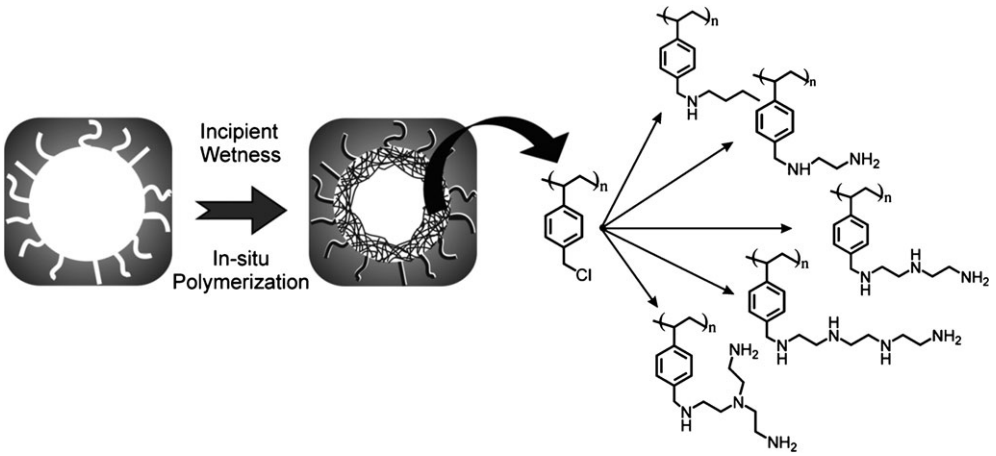

Scheme 1 Representation of the incorporation of PCMS and subsequent covalent attachment of amines inside large pore mesoporous silica (SBA-15-type).

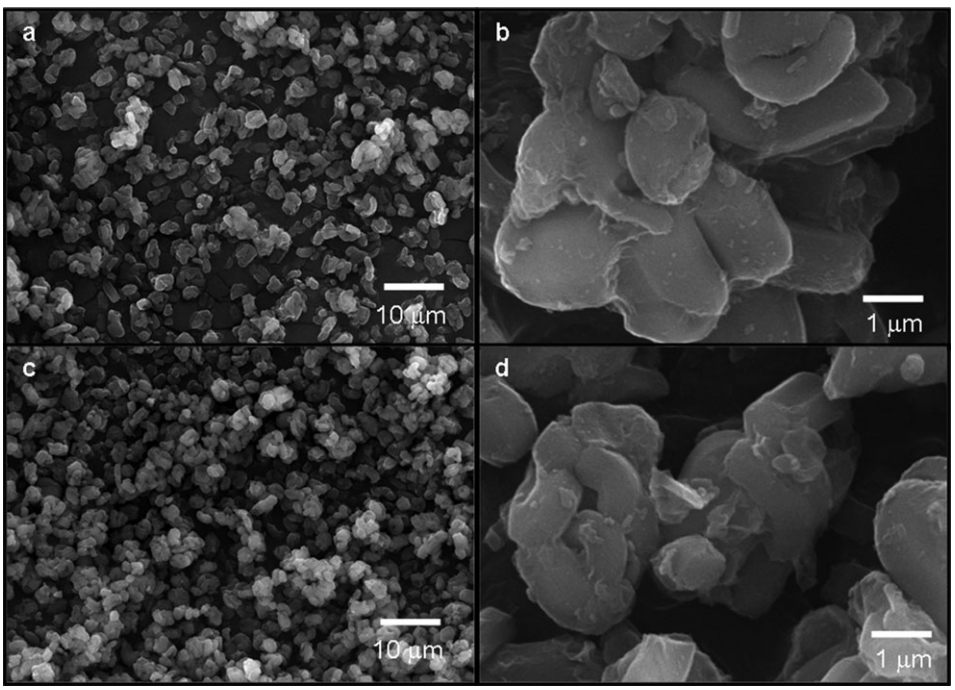

Fig. 3 Representative SEM images of PCMS(30)–SBA-15 (a) and (b), and EDA–PCMS(30)–SBA-15 (c) and (d).

observed for the composites (Table 1). The presence of 23 wt% of PCMS (30 wt% relative to the mass of SBA-15) leads to a pore size reduction of about 1.0 nm according to both NLDFT and BJH methods, corresponding to twice the thickness of the polymer coating, *i.e.* 0.5 nm in this case. Pore size reduction correlates well with the weight loading of PCMS in the composite, as also viewed in Fig. 5. In the composite with 10 wt% loading, the pore size is reduced by only 0.2 nm, which is slightly less than one third of what is observed for the 30 wt% composite. Note that the NLDFT kernel chosen for the pore size analysis considers interaction potentials involving pure silica surface and nitrogen at −196 °C, which should be viewed as an approximation in the case of the silica–polymer composites. Nevertheless, the influence of the adsorption potential on pore condensation[59] in the pore size regime considered above 5 nm is less critical, which is supported by a good agreement between the experimental isotherm and the NLDFT curve in the relative pressure range corresponding to the hysteresis loop (fit not shown). Up to 30 wt%, the resulting polymer–SBA-15 nanocomposite remains highly porous with easily accessible mesopores. A further increase in polymer loading from 30 to 40 wt% inside SBA-15 leads to a loss of the H1 character of the hysteresis loop (Fig. 4) suggesting pore blocking, *i.e.* constrictions due to the non-uniform PCMS coating. The effect is becoming increasingly pronounced for a 50 wt% loading (not shown). In general, similar trends are observed when introducing PCMS inside the pores of KIT-6, *i.e.* a reduction in pore size, pore volume and surface area. However, according to data presented in Table 1 and Fig. 5, a pore diameter reduction of only 0.7 nm (NLDFT equilibrium

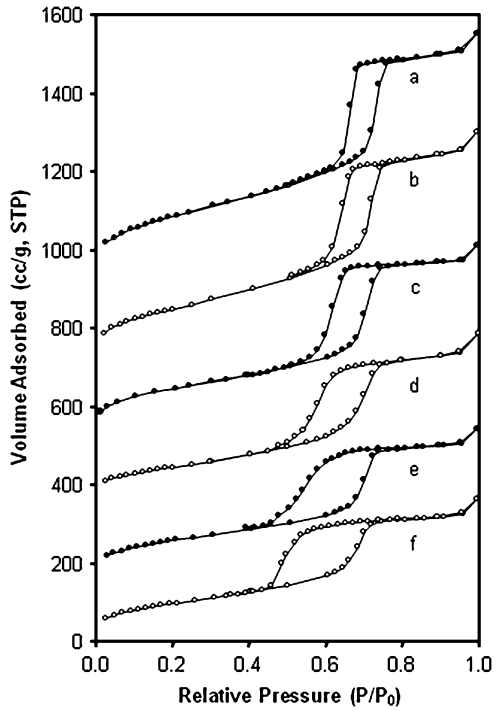

Fig. 4 N_2 adsorption–desorption isotherms measured at −196 °C for (a) PCMS(10)–SBA-15; (b) EDA–PCMS(10)–SBA-15; (c) PCMS(30)–SBA-15; (d) EDA–PCMS(30)–SBA-15; (e) PCMS(40)–SBA-15 and (f) EDA–PCMS(40)–SBA-15. Isotherms are offset by 900, 700, 500, 350 and 150 $cm^3\ g^{-1}$, respectively.

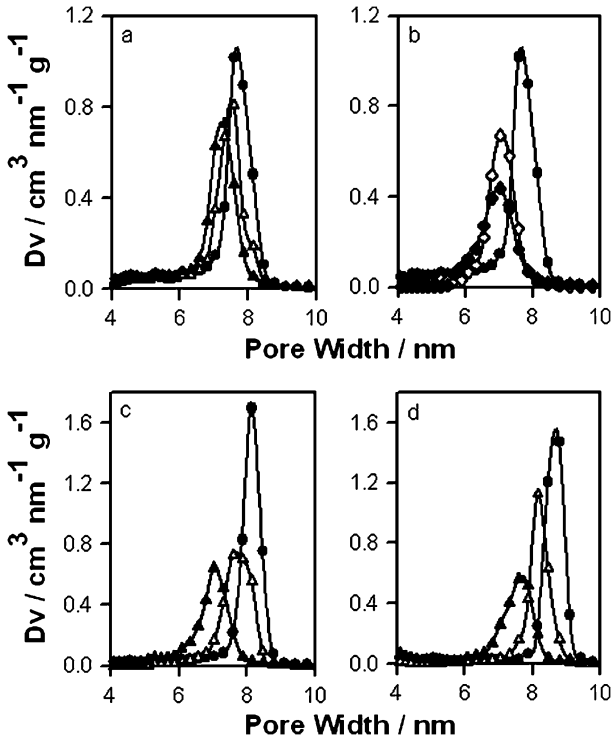

Fig. 5 NLDFT pore size distributions for: (a) and (b) SBA-15 silica (●), PCMS(10)–SBA-15 (△), EDA–PCMS(10)–SBA-15 (▲), PCMS(30)–SBA-15 (◇) and EDA–PCMS(30)–SBA-15 (♦); (c) and (d) KIT-6 silica (●), PCMS(30)–KIT-6 (△) and EDA–PCMS(30)–KIT-6 (▲). Data are all obtained applying the kernel of NLDFT metastable adsorption isotherms (adsorption branch), except for (d) obtained by applying the kernel of NLDFT equilibrium isotherms (desorption branch).

model) is caused by the introduction of 30 wt% PCMS in the KIT-6 silica matrix despite similar polymer content in the material. This suggests that the polymer location/distribution could be slightly different when comparing the two host materials. Differences between SBA-15 and KIT-6 in terms of total pore volume and/or volume of the intrawall pores (micropores–mesopores) might explain these variations.

Amination of the PCMS–SBA-15 nanocomposites

Reaction of the PCMS–SBA-15 composites with a diluted acetonitrile solution of an amine, *e.g.* ethylenediamine, is suitable to introduce amine functional groups onto the mesopore surface of the materials (Scheme 1). This method is derived from classical techniques applied for the amination of bulk polymers.[56,57] A control of the amount of functional groups (nitrogen groups) introduced in the material is in principle possible by adjusting the amount of reactive polymer in the composite. The N_2 sorption isotherms of three different PCMS–SBA-15 samples (10, 30 and 40 wt%) after reaction with ethylenediamine are shown in Fig. 4. The physicochemical characteristics of the obtained aminated materials are found in Table 1. In each case, the reaction with EDA leads to a systematic reduction in pore size, pore volume and surface area, suggesting that EDA has successfully been inserted inside the pores of the mesoporous PCMS–silica composites. EDA–PCMS(30) contains 2.1 mmol of nitrogen per gram of composite, which is close to the calculated theoretical value of 2.3 mmol g^{-1} and compares to data obtained using different approaches.[34,38] The treatment with EDA in acetonitrile seems not to affect greatly the situation of the occluded polymer, which remains stable under these conditions. However, the nitrogen sorption hysteresis loop becomes noticeably wider after the amination step (Fig. 4). Consequently, the mean NLDFT pore size obtained from the desorption branch (NLDFT equilibrium model) is substantially lower than that extracted from the adsorption branch (NLDFT metastable adsorption branch model) (Table 1). This observed change in hysteresis behavior tends to confirm that the reaction occurred inside the mesopores of the PCMS–SBA-15 composites. One may suggest that the addition of the EDA chains anchored at the surface of the polymer could induce changes in the pore surface with more corrugations at the pore entrances leading to a deviation from the ideal cylindrical geometry. Concerning KIT-6, the treatment of PCMS(30)–KIT-6 with EDA leads to a reduction in pore size of about 0.5 nm. However, no delayed desorption is occurring in this case with the hysteresis loop remaining narrow. This observation is significant because it suggests that the more open and totally interconnected pore network structure of the KIT-6 matrix could prevent any effects of pore corrugation, otherwise inducing delayed desorption (Fig. S1, ESI†).

Varying the PCMS initial loading from 10% to 40% leads to a variation in amine content from 1.0 mmol g^{-1} to 2.6 mmol g^{-1} (Table 1). A further increase in PCMS to 50%

does not allow generating a higher amine content, most likely because of a lower site accessibility in thicker polymer layers. Also, high loadings induce a more pronounced pore blocking effect and may be detrimental for applications requiring easy access to the functional groups. It is furthermore observed that a three-fold reduction in polymer loading results in a two-fold reduction in the total nitrogen content. One may here suggest that a 10% polymer loading might not be sufficient to cover completely the inside of the mesopore channels, thus leaving a substantial amount of free silanol accessible on the pore surface for direct anchoring of excess EDA moieties. This hypothesis would be in line with conclusions made recently by Rosenholm *et al.*[20] in the case of poly(methacrylic acid)–SBA-15 composites.

The TG-DTA/MS data obtained for the composites at different stages of the functionalization process provide evidence of effective nucleophilic substitution of chlorine for the amine. The TG data obtained for PCMS (30 wt%) in SBA-15 show a substantial weight loss of 23%, indicative of the presence of the organic polymer (Fig. 6 and Fig. S2 (ESI†) for the respective DTA curves). The DTA signal for the same composite prior to amination indicates two exothermic degradation processes starting at 250 °C, with maxima occurring at 350 °C and 600 °C. These processes are characteristic of cross-linked polystyrene, and may be associated with the formation of primary char, further followed by degradation at higher temperatures.[66,67] Treatment of PCMS(30) with EDA leads to only 2% increase in the organic content (from 23% to 25.2%). Also, a weak additional DTA effect centered at 250 °C is visible. The most intense peak related to chlorine in the MS spectra, $m/z = 36$ (corresponding to the HCl^+ species), almost disappeared after treatment with EDA, as shown in Fig. 6. Furthermore, a noticeable increase of the $m/z = 30$ trace, assigned to $C_2H_6^+$ from EDA moieties, is being consistent with the replacement of the majority of chlorine atoms by EDA chains in the materials. Hence, a large fraction of the chlorine groups seems to be available for substitution with the EDA molecules. Considering the high degree of cross-linking applied during polymer synthesis (20%), one could attribute this high accessibility of the reactive sites to the thin homogeneous polymer surface coating, affording polymeric functionalities with high surface area (300–600 $cm^3\ g^{-1}$). The exothermic effect present after EDA introduction seems to be associated to the release of water, since the only species detected in MS below 250 °C is H_2O ($m/z = 18$). It is however not possible at this stage to exclude a contribution from the decomposition of amines (*e.g.* NH_3^+, NH_4^+ species). The introduction of EDA moieties in the composites is further confirmed by IR spectroscopy. The ATR-IR spectra of pristine SBA-15 and the different composites are presented in Fig. 7. The graph *a* shows the typical peaks observed for silica in the region shown: a strong absorbance band at 3748 cm^{-1} assigned to free Si–OH stretching, a wide band between 3700 and 2950 cm^{-1} and a sharper one at 1628 cm^{-1} attributed to the presence of adsorbed water on silanols. The presence of PCMS introduces new absorbance bands, with the more important ones at 2980 and 2930 cm^{-1} caused by CH symmetric and asymmetric stretching. A noticeable decrease in intensity of the SiOH band (3748 cm^{-1}) is observed upon PCMS incorporation. The introduction of amines is judged by the presence of N–H stretching bands at 3350 and 3250 cm^{-1} and bending at 1507 cm^{-1}. Another band associated with the CH_2 stretching is also visible at 2850 cm^{-1}, and the existing CH stretching bands gain in intensity. In addition to a decreased fraction of silica in the material, the reduction in intensity of the Si–OH band indicates that some functional groups could interact with free surface Si–OH groups, in particular, amines may be directly linked to the silica surface *via* H-bonding interactions. In addition, the aromatic ring of CMS moieties may also be weakly interacting with silanol groups.[64,68] The ATR-FTIR

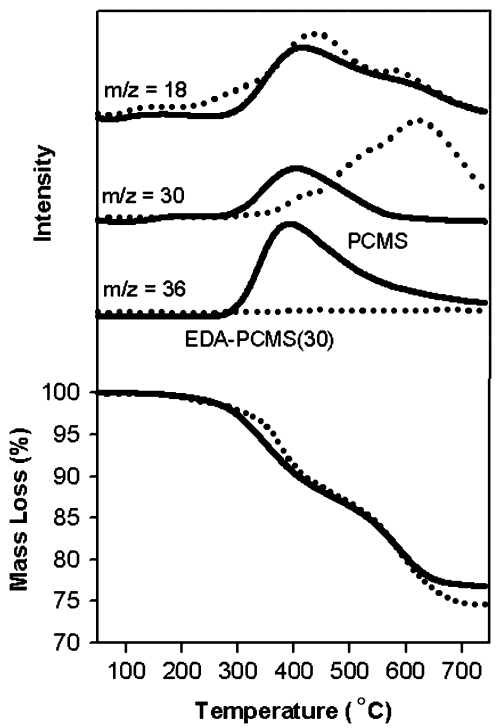

Fig. 6 TGA weight loss profiles and associated MS traces for the PCMS(30)–SBA-15 composite before and after amination (solid line: PCMS(30)–SBA-15, dotted line: EDA–PCMS(30)–SBA-15).

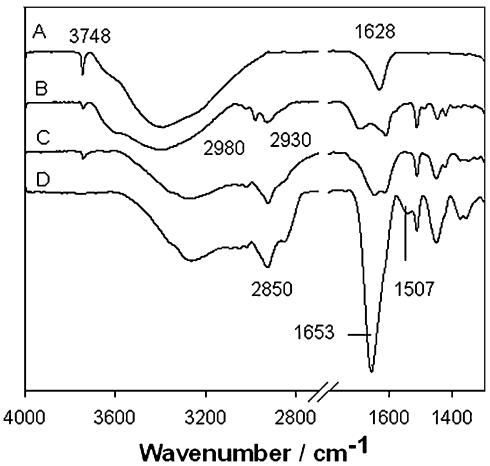

Fig. 7 ATR-FTIR spectra of (A) SBA-15, (B) PCMS(30)–SBA-15, (C) EDA–PCMS(30)–SBA-15 and (D) TAEA–PCMS(30)–SBA-15.

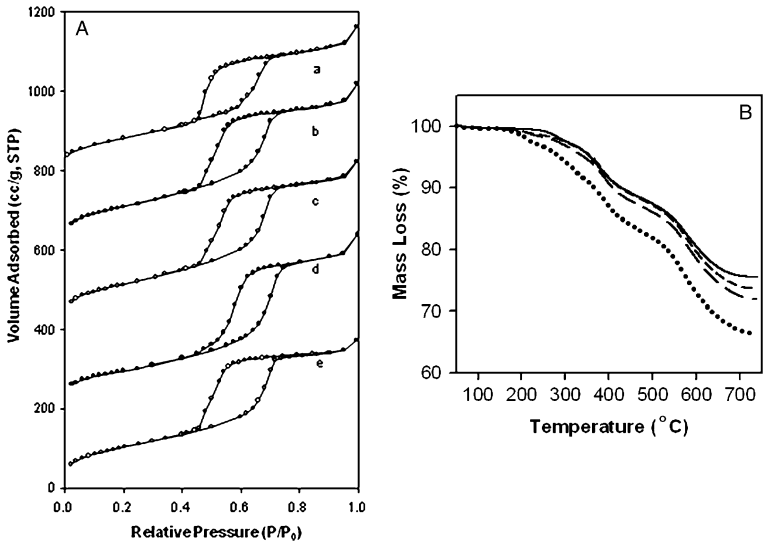

Fig. 8 (A) N_2 sorption isotherms of amino-functionalized polymer–silica composites using different amines (a) TAEA; (b) TETA; (c) DETA; (d) EDA; (e) BA. Offsets are 800, 600, 400 and 200 $cm^3\ g^{-1}$, respectively. (B) TG analysis of PCMS–SBA-15 composites treated with BA (solid), DETA (short dash), TETA (long dash) and TAEA (dotted).

Physicochemical parameters for polymer–silica composites with different grafted amines

Grafted amine	BET/ $m^2\ g^{-1}$	Pore volume[a]/$cm^3\ g^{-1}$	DFT pore size[b]/nm	DFT pore size[c]/nm	Organic content[d]/wt%	N content[e]/mmol g^{-1} Theo.	N content[e]/mmol g^{-1} Expt.	Substitution (%)
TAEA	302	0.50	5.5	6.6	33.2	4.4	4.1	93
TETA	401	0.58	5.7	6.8	27.7	4.4	2.9	66
DETA	421	0.60	5.7	6.8	25.9	3.5	2.0	57
EDA	351	0.61	6.3	7.0	25.2	2.3	2.1	91
BA	386	0.54	5.5	6.8	24.2	1.2	0.7	58

[a] Determined at $P/P_0 = 0.95$. [b] Determined by NLDFT method taking into account the desorption branch (NLDFT equilibrium model). [c] Determined by NLDFT method taking into account the adsorption branch (NLDFT metastable adsorption branch model). [d] Obtained by TG. [e] Determined by combustion elemental analysis.

spectra recorded for the KIT-6 series show similar features (see Fig. S3A, ESI†).

In the following, emphasis is put on materials obtained using SBA-15 as the host, samples prepared with KIT-6 silica being in general quite comparable. The technique employed to attach EDA moieties on PCMS–SBA-15 composites was extended to introduce varieties of amines. For instance, tris(2-aminoethyl)amine, TAEA, triethylenetetramine, TETA, diethylenetriamine, DETA and butylamine, BA, moieties have also been incorporated into the mesoporous silica–polymer composites. Nitrogen physisorption isotherms and physicochemical parameters of these different amino-functionalized mesoporous materials are shown in Fig. 8A and Table 2. The materials resulting from the reaction with DETA and TETA exhibit a type IV isotherm with H1 hysteresis loop, characteristic of capillary condensation in cylindrical mesopores. However, in the case of TAEA and BA, a wider H2 type hysteresis loop is observed, signifying pronounced pore blockage upon insertion of bulkier amine groups. Here, the shape of the mesopores might thus be considered as being closer to ink-bottle-like pores. Similar to EDA, reaction of PCMS–SBA-15 with the different amines leads generally to systematic reduction in pore volume, pore size and surface area, reflecting efficient functionalization inside the mesopores. The total organic content and nitrogen content determined by TG analyses and CHN combustion analyses, respectively, are compiled in Fig. 8B and in Table 2. Using different amines, the total nitrogen content could be varied from 0.7 to up to 4.1 mmol g^{-1}, the highest value being for the TAEA-based composite (4.1 mmol g^{-1} and 33.2 wt% of polymer), which corresponds to a 93% chlorine substitution fraction. Note that the EDA–PCMS composite also showed similarly high chlorine substitution yield (91%). These values contrast with those calculated for the three other composites, for which the organic and nitrogen contents are significantly lower (Fig. 8B and Table 2). In the case of BA, the lower substitution may be explained in terms of lower reactivity of the alkylmonoamine compared to the diamine (EDA). In the cases of DETA and TETA, the length of the molecule might induce steric hindrance limiting the substitution. A similar behavior would, however, be expected for TAEA, but high substitution yield is obtained, possibly owing to the presence of three primary amine groups in this molecule. The ATR-IR spectrum of TAEA-PCMS on Fig. 7 shows pronounced reduction in intensity of the free SiOH band (3748 cm^{-1}) as compared to PCMS–SBA-15, which is also pointing to interactions between TAEA and silanols which had remained accessible. An additional interesting feature is the presence of a strong

absorbance band at 1653 cm^{-1}, most likely associated with the presence of adsorbed CO_2.[43,44,69] This band is stronger for the TAEA composite, confirming that CO_2 sorption correlates with the nitrogen content.

Surface polarity could have an important impact on the activity of a catalyst or a sorbent.[70] Consequently, in an attempt to tailor the hydrophilic–hydrophobic environment of the amine groups, the CMS monomer was copolymerized with a non-reactive monomer, *i.e.* styrene. By controlling the amount of chloromethylstyrene and styrene initially introduced by impregnation, *i.e.* different CMS/S ratios, it should in principle be possible to tune amount, density and surface coverage of functional groups at the pore surface. The physicochemical characteristics of the different PCMS/PS–SBA-15 composites synthesized (CMS/S = 1 : 1 and 1 : 10) are summarized in Table 1. Before amination, the different copolymer composites exhibit rather similar pore size (~7.0–7.3 nm, NLDFT metastable adsorption branch model), pore volume (~0.75–0.8 cm^3 g^{-1}) and surface area (~500 m^2 g^{-1}). The copolymer-based materials obtained after insertion of EDA exhibit specific surface area over 400 m^2 g^{-1} and similar pore size around 6.8–7.3 nm (NLDFT metastable adsorption). Nitrogen physisorption isotherms are shown in Fig. S4.† Noticeable is the fact that the hysteresis widths of the isotherms are quite different for materials prepared with 10% and 50% CMS, with the lower CMS content leading to a narrower hysteresis loop. This difference might originate from the fact that much less amine chains are present in the PCMS(0.1; 30) copolymer composite. As expected, the aminated copolymer–SBA-15 composites exhibit different nitrogen content, being 2.1, 1.3 and 0.6 mmol g^{-1} for EDA–PCMS(1; 30)–SBA-15, EDA–PCMS(0.5; 30)–SBA-15 and EDA–PCMS(0.1; 30)–SBA-15, respectively. The amine content is related to the PCMS fraction but no clear linear relationship was evidenced, possibly due to the anchoring of excess EDA species directly on accessible silanol groups. The ATR-IR spectra show an increasing contribution of peaks related to the presence of EDA moieties with higher nitrogen content in the copolymers (Fig. S3B, ESI†). However, no distinct peak broadening effect, which would be related to heterogeneity in the amine sites[71] is visible in these spectra.

To further confirm the location of the amine-functionalized polymer coating, the EDA–PCMS(30)–SBA-15 composite was compared with materials prepared with two different polymer locations, *i.e.* a randomly incorporated polymer and a physical mixture of EDA–PCMS and SBA-15. All the three materials exhibit similar polymer content as judged from comparable weight loss profiles. The polymer location is evidenced by N_2 sorption, as shown in Fig. 9. Compared to the coated composite material, the random composite exhibits a H2 type hysteresis, which is characteristic of ink-bottle pores and indicative of the presence of constrictions and pronounced pore blocking effects. The hysteresis of the random composite suggests the phenomenon of cavitation, *i.e.* spontaneous desorption of nitrogen from the mesopores, consequence of the presence of small pore necks.[72] This clearly indicates that the polymer is present inside the pores not as a coating, but as a random heterogeneous filling. These random and coated materials both exhibit substantially reduced surface area and pore volume, supporting that the polymer was indeed placed inside the pores of the parent silica host. In contrast, higher surface area and pore volume are obtained for the composite based on a physical mixture, which implies that the porous network is still fairly available. Here, the hysteresis loop does not differ much from that of the parent SBA-15, indicating that no polymer is present in the pores. Furthermore, one can see from Table S2 (ESI†) that very similar NLDFT pore size values are obtained for the physical mixture and the pristine SBA-15, being 7.8 and 8.1 nm for the physical mixture (from adsorption and desorption branches, respectively). Additionally, the different isotherms were recalculated taking into account the mass of silica only (Table S2, ESI†). The thus-obtained sorption values for the physical mixture are very close to those of the pure silica SBA-15, confirming that the polymer is in this case located outside of the porous network. In contrast, recalculated BET surface area and pore volume for the two other composites are still about 300 m^2 g^{-1} and 0.30 cm^3 g^{-1} lower than those obtained from the initial

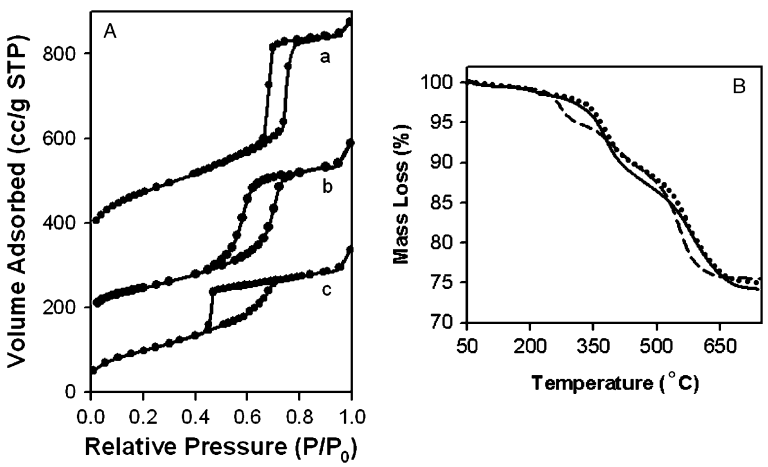

Fig. 9 (A) N_2 sorption isotherms of EDA–PCMS composites with different polymer locations: (a) physical mixture, (b) coated EDA–PCMS(30)–SBA-15, and (c) random (EDA–PCMS(30)-R–SBA-15). Offsets are 300 and 150 cm^3 g^{-1}, respectively. (B) TGA curves for EDA–PCMS composites with different polymer locations: coated (solid); random (dotted) and physical mixture (dashed).

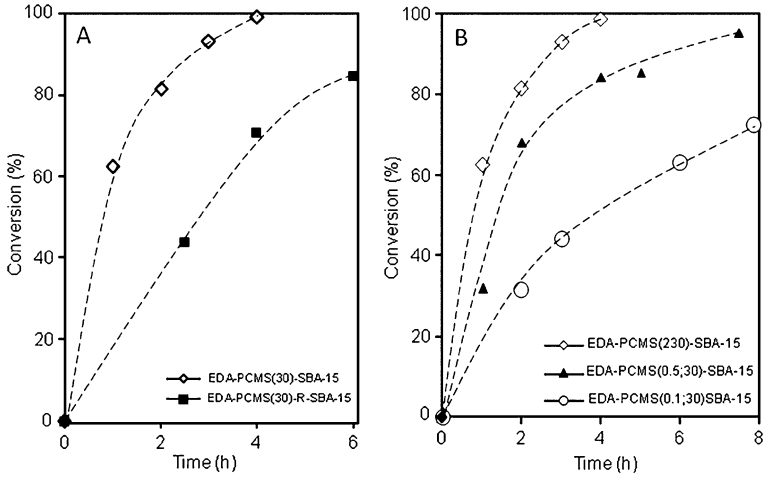

Fig. 10 Time-course of the Knoevenagel condensation of benzaldehyde with ethyl cyanoacetate catalyzed by: (A) ◇ EDA–PCMS(30)–SBA-15; ■ EDA–PCMS(30)-R–SBA-15; and (B) ◇ EDA–PCMS(30)–SBA-15; ▲ EDA–PCMS(0.5; 30)–SBA-15; ○ EDA–PCMS(0.1; 30). The reaction was carried out with equimolar mixture (5 mmol) of benzaldehyde and ethyl cyanoacetate in 35 mL toluene at 80 °C.

SBA-15 material, confirming that the polymer is present inside the pores of SBA-15.

A series of comparative catalytic tests were conducted with different EDA-functionalized composites prepared with 30 wt% of polymer. The composites were evaluated for the Knoevenagel condensation of benzaldehyde with ethyl cyanoacetate, which is a typical test reaction.[70] Conversions of benzaldehyde (5 mmol) to ethyl α-cyanocinnamate are plotted as a function of time for 50 mg of catalyst prepared by the above different approaches (Fig. 10). For EDA–PCMS(30)–SBA-15, complete conversion is achieved within 4 h, and no other products than ethyl α-cyanocinnamate are observed, which compare well with some of the most active amino-functionalized silica catalysts reported.[38,39] The productivity, which we define as the amount of ethyl α-cyanocinnamate formed per mass of catalyst as a function of time, is 38 mol mg_{cat}^{-1} h^{-1} for this catalyst. In addition, the productivity relative to the amine content (obtained from elemental analysis) is 0.018 mol $mmol_{am}^{-1}$ h^{-1}. The randomly incorporated polymer–SBA-15 material, EDA–PCMS(30)-R, obviously exhibits lower conversion over time and twice as low a productivity compared to the well-coated EDA–PCMS(30)–SBA-15 equivalent, *i.e.* 17 mol mg_{cat}^{-1} h^{-1}. Problems of accessibility caused by pore blocking or less exposed active sites may be the cause for the lower activity of the random composite. In other words, uniformity of the polymer coating is a prerequisite for higher catalytic activity. As expected, a decrease of the amine content by performing copolymerization results in a decrease in the catalytic activity for a similar mass. However, the correlation is not linear: after a 2 h period, EDA–PCMS(0.5; 30) and (0.1; 30) show conversions of 68% and 32%, respectively, as compared to 82% for EDA–PCMS(30) (Fig. 10B). In terms of productivity per mass, the value of 38 mol mg_{cat}^{-1} h^{-1} for EDA–PCMS(30) is only diminished to 34 mol mg_{cat}^{-1} h^{-1} for EDA–PCMS(0.5; 30), despite an amine content corresponding to *ca.* 60% of the initial value. Here, a possibly lower density of amine groups on the pore surface in these *diluted* PCMS–PS composites and/or less polar polymer environments[70,73] might be beneficial for higher activity per catalytic site (productivity). A further reduction in the CMS fraction, which causes the nitrogen content to decrease from 1.3 to 0.6 mmol g^{-1} (a 54% reduction), leads to a drop in productivity down to 16 mol mg_{cat}^{-1} h^{-1}. Such effects are even more pronounced when catalytic activity relative to amine content is considered. EDA–PCMS(0.5; 30) and (0.1; 30) exhibit the same molar productivity, *i.e.* 0.026 mol $mmol_{am}^{-1}$ h^{-1}, which is superior to that calculated for EDA–PCMS(30), *e.g.* 0.018 mol $mmol_{am}^{-1}$ h^{-1}. Note that the decrease of amine-to-reagent ratio (from 2% to 0.5%) by lowering the mass of the catalyst (for EDA–PCMS(30)–SBA-15) resulted in a decrease in conversion proportional to the mass used, as expected (Fig. S5, ESI†). Recycling of the catalysts has also been tested, the results being shown in Table S3.† The decreasing productivity upon repeated use indicates that all the catalysts investigated in this study deactivate markedly, with about a two-fold decrease observed at each re-utilization. However, elemental analysis revealed that no leaching is observed during reaction and the reaction does not proceed further if the catalyst is removed by hot filtration. Such a deactivation process has also been observed previously for aminated MCM-41 materials and discussed by Macquarrie *et al.*[36,70] From these studies, one could suggest that irreversible formation of amide on the surface when reacting with ethyl cyanoacetate or, alternatively, the formation of $-NH_3^+$ ^-O_2CR salts, caused by possible reaction with CO_2 from air,[74] may be some sources of deactivation. Wang *et al.*[38] suggested the possibility of regeneration by a simple basic treatment with tetramethylammonium hydroxide in methanol solution. However, we experienced limited success in using this approach for the EDA–PCMS composites.

Conclusions

Pore surface-confined polymerization followed by post-functionalization is a versatile technique for introducing various functional amines into large pore mesoporous silica and to tune, to some extent, their chemical environment. With this method, ordered mesoporous composites with nitrogen

content ranging from 0.6 to 4.1 mmol g^{-1} were synthesized by using different amines and varying the initial polymer loading. The results support covalent attachment of the amine species into the polymer layers present inside the pores. Furthermore, copolymerization of CMS with styrene allowed additional tailoring of the amine content and, most likely, the amine surface density. In addition, differences between composites synthesized from SBA-15 and KIT-6 hosts were revealed, with the remarkable absence of pore blocking effect in the case of KIT-6. The materials are shown to be active as catalysts in the Knoevenagel condensation reaction confirming their potential in liquid phase heterogeneous catalysis. However, a comparison with other existing amino-functionalized mesoporous materials regarding activity and selectivity in different catalytic systems is still required to determine whether the above nanoporous composites have real perspectives of application in catalysis. In relation to this, further investigations are ongoing in order to compare different amino-polymer composites (prepared with various hosts, with different amines, or with modulated surface environments) with some reference materials synthesized by grafting or co-condensation methods; and the results of these studies will be reported shortly. Nevertheless, because the mesopore polymer coating method only requires simple and low-cost organic molecules for the surface modification, we believe that it may easily be adapted further to a vast variety of organic species opening therefore access to almost unlimited functionalization possibilities.

Acknowledgements

Financial supports from the Natural Sciences and Engineering Research Council of Canada (NSERC) and le Fonds Québécois de la Recherche sur la Nature et les Technologies (FQRNT) are gratefully acknowledged. The authors wish to thank Prof. Michel Pézolet and Jean-François Rioux for the access to ATR-IR measurements (Department of Chemistry, Université Laval).

References

1 J. S. Beck, J. C. Vartuli, W. J. Roth, M. E. Leonowicz, C. T. Kresge, K. D. Schmitt, C. T. W. Chu, D. H. Olson, E. W. Sheppard, S. B. McCullen, J. B. Higgins and J. L. Schlenker, *J. Am. Chem. Soc.*, 1992, **114**, 10834.
2 D. Zhao, Q. Huo, J. Feng, B. F. Chmelka and G. D. Stucky, *J. Am. Chem. Soc.*, 1998, **120**, 6024.
3 Y. Wan and D. Y. Zhao, *Chem. Rev.*, 2007, **107**, 2821.
4 A. Taguchi and F. Schüth, *Microporous Mesoporous Mater.*, 2005, **77**, 1.
5 J. Y. Ying, C. P. Mehnert and M. S. Wong, *Angew. Chem., Int. Ed.*, 1999, **38**, 56.
6 M. Vallet-Regi, F. Balas and D. Arcos, *Angew. Chem., Int. Ed.*, 2007, **46**, 7548.
7 M. Tiemann, *Chem.–Eur. J.*, 2007, **13**, 8376.
8 M. Hartmann, *Chem. Mater.*, 2005, **17**, 4577.
9 J. H. Clark and D. J. Macquarrie, *Chem. Commun.*, 1998, 853.
10 A. P. Wight and M. E. Davis, *Chem. Rev.*, 2002, **102**, 3589.
11 G. Kickelbick, *Angew. Chem., Int. Ed.*, 2004, **43**, 3102.
12 H. Yoshitake, *New J. Chem.*, 2005, **29**, 1107.
13 F. Hoffmann, M. Cornelius, J. Morell and M. Fröba, *Angew. Chem., Int. Ed.*, 2006, **45**, 3216.
14 D. M. Ford, E. E. Simanek and D. F. Shantz, *Nanotechnology*, 2005, **16**, S458.
15 M. Choi, F. Kleitz, D. Liu, H. Y. Lee, W. S. Ahn and R. Ryoo, *J. Am. Chem. Soc.*, 2005, **127**, 1924.
16 M. Choi and R. Ryoo, *Nat. Mater.*, 2003, **2**, 473.
17 L. Zhang, H. C. L. Abbenhuis, G. Gerritsen, N. N. Bhriain, P. C. M. M. Magusin, B. Mezari, W. Han, R. A. van Santen, Q. Yang and C. Li, *Chem.–Eur. J.*, 2007, **13**, 1210.
18 P. M. Arnal, F. Schüth and F. Kleitz, *Chem. Commun.*, 2006, 1203.
19 Y. Zhang, L. Zhao, S. S. Lee and J. Y. Ying, *Adv. Synth. Catal.*, 2006, **348**, 2027.
20 J. M. Rosenholm, T. Czuryszkiewicz, F. Kleitz, J. B. Rosenholm and M. Lindén, *Langmuir*, 2007, **23**, 4315.
21 (*a*) J. Moreno and D. C. Sherrington, *Chem. Mater.*, 2008, **20**, 4468; (*b*) M. Kruk, B. Dufour, E. Celer, T. Kowalewski, M. Jaroniec and K. Matyjaszewski, *Macromolecules*, 2008, **41**, 8544; (*c*) J. D. Lunn and D. Shantz, *Chem. Mater.*, 2009, **21**, 3638.
22 B. S. Tian and C. Yang, *J. Phys. Chem. C*, 2009, **113**, 4925.
23 C. C. Wu and T. Bein, *Science*, 1994, **264**, 1757.
24 K. Moller, T. Bein and R. X. Fischer, *Chem. Mater.*, 1998, **10**, 1841.
25 M. S. Cho, H. J. Choi, K. Y. Kim and W. S. Ahn, *Macromol. Rapid Commun.*, 2002, **123**, 713.
26 X. C. Xu, C. S. Song, J. M. Andresen, B. G. Miller and A. W. Scaroni, *Energy Fuels*, 2002, **16**, 1463.
27 A. G. Pattantyus-Abraham and M. O. Wolf, *Chem. Mater.*, 2004, **16**, 2180.
28 E. J. Acosta, C. S. Carr, E. E. Simanek and D. F. Shantz, *Adv. Mater.*, 2004, **16**, 985.
29 W. C. Molenkamp, M. Watanabe, H. Miyata and S. H. Tolbert, *J. Am. Chem. Soc.*, 2004, **126**, 4476.
30 J. M. Rosenholm, A. Penninkangas and M. Lindén, *Chem. Commun.*, 2006, 3909.
31 M. Save, G. Granvorka, J. Bernard, B. Charleux, C. Boissiere, D. Grosso and C. Sanchez, *Macromol. Rapid Commun.*, 2006, **27**, 393.
32 F. Kleitz, S. H. Choi and R. Ryoo, *Chem. Commun.*, 2003, 2136.
33 Y. V. Subba Rao, D. E. DeVos and P. A. Jacobs, *Angew. Chem., Int. Ed. Engl.*, 1997, **36**, 2661.
34 T. Yokoi, H. Yoshitake, T. Yamada, Y. Kubota and T. J. Tatsumi, *J. Mater. Chem.*, 2006, **16**, 1125.
35 Y. Xia and R. Mokaya, *Angew. Chem., Int. Ed.*, 2003, **42**, 2639.
36 D. J. Macquarrie and D. B. Jackson, *Chem. Commun.*, 1997, 1781.
37 Y. Inaki, Y. Kajita, H. Yoshida, K. Ito and T. Hattori, *Chem. Commun.*, 2001, 2358.
38 (*a*) X. Wang, K. S. K. Lin, J. C. C. Chan and S. Cheng, *J. Phys. Chem. B*, 2005, **109**, 1763; (*b*) X. Wang, J. C. C. Chan, Y. H. Tseng and S. Cheng, *Microporous Mesoporous Mater.*, 2006, **95**, 57.
39 X. Wang, Y. H. Tseng, J. C. C. Chan and S. Cheng, *J. Catal.*, 2005, **233**, 266.
40 J. H. Huang, G. Tian, H. S. Wang, L. Xu and Q. B. Kan, *J. Mol. Catal. A: Chem.*, 2007, **271**, 200.
41 J. E. G. Mdoe, J. H. Clark and D. J. Macquarrie, *Synlett*, 1998, 625.
42 B. M. Choudary, M. L. Kantam, P. Sreekanth, T. Bendopadhyay, F. Figueras and A. Tuel, *J. Mol. Catal. A: Chem.*, 1999, **142**, 361.
43 A. C. C. Chang, S. S. C. Chuang, M. Gray and Y. Soong, *Energy Fuels*, 2003, **17**, 468.
44 F. Zheng, D. N. Tran, B. J. Busche, G. E. Fryxell, R. S. Addleman, Z. S. Zemanian and C. L. Aardahl, *Ind. Eng. Chem. Res.*, 2005, **44**, 3099.
45 S. Kim, J. Ida, V. V. Guliants and J. Y. S. Lin, *J. Phys. Chem. B*, 2005, **109**, 6287.
46 X. Feng, G. E. Fryxwell, L. Q. Wang, A. Y. Kim, J. Liu and K. M. Kemner, *Science*, 1997, **276**, 923.
47 H. Yoshitake, E. Koiso, H. Horie and H. Yoshimura, *Microporous Mesoporous Mater.*, 2005, **85**, 183.
48 K. McEleney, D. P. Allen, A. E. Holliday and C. M. Crudden, *Org. Lett.*, 2006, **8**, 2663.
49 S. W. Song, K. Hidajat and S. Kawi, *Langmuir*, 2005, **21**, 9568.
50 Z. J. Wu, Y. Jiang, T. H. Kim and K. T. Lee, *J. Controlled Release*, 2007, **119**, 215.
51 J. M. Rosenholm and M. Lindén, *J. Controlled Release*, 2008, **128**, 157.
52 (*a*) J. M. Rosenholm, A. Meinander, E. Peuhu, R. Niemi, J. E. Eriksson, C. Sahlgren and M. Lindén, *ACS Nano*, 2009, **3**, 197; (*b*) J. M. Rosenholm, E. Peuhu, J. E. Eriksson, C. Sahlgren and M. Lindén, *Nano Lett.*, 2009, **9**, 3308.

53 M. Choi, W. Heo, F. Kleitz and R. Ryoo, *Chem. Commun.*, 2003, 1340.
54 T. W. Kim, F. Kleitz, B. Paul and R. Ryoo, *J. Am. Chem. Soc.*, 2005, **127**, 7601.
55 A. Diaf, J. L. Garcia and E. J. Beckman, *React. Funct. Polymers*, 1995, **27**, 45.
56 P. Krajnc, J. F. Brown and N. R. Cameron, *Org. Lett.*, 2002, **4**, 2497.
57 A. Diaf, J. L. Garcia and E. J. Beckman, *J. Appl. Polym. Sci.*, 1994, **53**, 857.
58 P. I. Ravikovitch and A. V. Neimark, *J. Phys. Chem. B*, 2001, **105**, 6817.
59 M. Thommes, in *Nanoporous Materials; Science and Engineering*, ed. G. Q. Lu and X. S. Zhao, Imperial College Press, London, UK, 2004, pp. 317–364.
60 A. V. Neimark and P. I. Ravikovitch, *Microporous Mesoporous Mater.*, 2001, **44**, 697.
61 A. Galarneau, N. Cambon, F. Di Renzo, R. Ryoo, M. Choi and F. Fajula, *New J. Chem.*, 2003, **27**, 73.
62 F. Kleitz, T. W. Kim and R. Ryoo, *Langmuir*, 2006, **22**, 440.
63 R. Guillet-Nicolas, F. Bérubé and F. Kleitz, *Stud. Surf. Sci. Catal.*, 2008, **174**, 141.
64 M. Wainer, L. Marcoux and F. Kleitz, *J. Mater. Sci.*, 2009, **44**, 6538.
65 M. Kruk, M. Jaroniec, C. H. Ko and R. Ryoo, *Chem. Mater.*, 2000, **12**, 1961.
66 G. F. Levchik, K. Si, S. V. Levchik, G. Camino and C. A. Wilkie, *Polym. Degrad. Stab.*, 1999, **65**, 395.
67 D. W. Van Krevelen, *Polymer*, 1975, **16**, 615.
68 B. Onida, M. Allian, E. Borello, P. Ugliengo and E. Garrone, *Langmuir*, 1997, **13**, 5107.
69 J. C. Hicks, J. H. Drese, D. J. Fauth, M. L. Gray, G. G. Qi and C. W. Jones, *J. Am. Chem. Soc.*, 2008, **130**, 2902.
70 J. H. Clarck, D. J. Macquarrie and S. J. Tavener, *Dalton Trans.*, 2006, 4297, and references therein.
71 B. A. McCool and W. J. DeSisto, *Adv. Funct. Mater.*, 2005, **15**, 1635.
72 (*a*) F. Kleitz, T. Czuryszkiewicz, L. A. Solovyov and M. Lindén, *Chem. Mater.*, 2006, **18**, 5070; (*b*) M. Thommes, B. Smarsly, M. Groenewolt, P. I. Ravikovitch and A. V. Neimark, *Langmuir*, 2006, **22**, 756.
73 D. J. Macquarrie, *Green Chem.*, 1999, **1**, 195.
74 G. Sartori, F. Bigi, R. Maggi, R. Sartorio, D. J. Macquarrie, M. Lenarda, L. Storaro, S. Coluccia and G. Martra, *J. Catal.*, 2004, **222**, 410.

